

# Effect of Wind Loads on Low-Rise Pitched and Circular Arch Roof Structures: A Comparative Study based on Numerical Simulation

Aditya Kumar Jha, Amartya Sinha, Ritu Raj\*

Department of Civil Engineering, Delhi Technological University, Delhi 110042, India

Received February 3, 2022; Revised March 4, 2022; Accepted April 15, 2022

## Cite This Paper in the following Citation Styles

(a): [1] Aditya Kumar Jha, Amartya Sinha, Ritu Raj, "Effect of Wind Loads on Low-Rise Pitched and Circular Arch Roof Structures: A Comparative Study based on Numerical Simulation," *Civil Engineering and Architecture*, Vol. 10, No. 3, pp. 1129-1141, 2022. DOI: 10.13189/cea.2022.100329.

(b): Aditya Kumar Jha, Amartya Sinha, Ritu Raj (2022). *Effect of Wind Loads on Low-Rise Pitched and Circular Arch Roof Structures: A Comparative Study based on Numerical Simulation*. *Civil Engineering and Architecture*, 10(3), 1129-1141. DOI: 10.13189/cea.2022.100329.

Copyright©2022 by authors, all rights reserved. Authors agree that this article remains permanently open access under the terms of the Creative Commons Attribution License 4.0 International License

**Abstract** Through numerical simulations based on Computational Fluid Dynamics (CFD), this study examines the effect of wind load operating on a pitched roof and a circular arch roof of an identical plan area of a storage structure with one wall opening. Many numerical simulations have been performed by other researchers for other types of roofs to understand the behavior of wind flow associated with them. Also, the wind standards of multiple countries have provided the Coefficients of Pressures for standard building shapes. However, there is lack of similar work for structures having one wall opening. Ansys CFX fluid flow software has been used to carry out the simulations using a standard k- $\epsilon$  turbulence model. The simulations have been carried out for 7 wind incidence angles at an interval of 30°. Pressure, Force, Moment, Drag and Lift Coefficients generated on the roofs were compared. It was found that, although variation in these coefficients w.r.t the wind incidence angles are similar for both the roofs types, the sharp-edged rooftop of the pitched roof contributes to higher magnitudes of these coefficients as compared to the smooth arch roof. Mathematical modules between the face average of pressure coefficients and the wind incidence angles were established in a polynomial form which could be used to find the face average of pressure coefficients and corresponding pressures and forces for arbitrary wind incidence angles.

**Keywords** Low Rise Structures, Pitched Roof, Arch

Roof, Ansys CFX, Wind Load, Pressure Coefficients

## 1. Introduction

The global economic expansion and large-scale industrialization have led to rising in the requirement of structures for storage facilities such as warehouses, godowns, cold storage, bunkers, structures like motor workshops, manufacturing units, etc. The air transportation network also plays an important role in facilitating rapid globalization. Hangars are key structures at airports that are used for aircraft repair, storage, and upkeep. These structures have large plan dimensions and involve truss roofs. The influence of wind on such roofs is enormous and needs to be critically analyzed. In recent years, various failures of such roof structures due to strong winds have occurred. In 2018, at Hobby airport in Huston, strong winds damaged the hangar roof damaging the parked planes.

The geometry of the roof and the slope of the roof are both important elements in the structure's wind load resistance. As a result, predicting wind loads on roofs is essential for building safe and cost-effective roof structures and trusses. With the use of computational fluid dynamics (CFD) simulations, wind load estimations may be done using numerical solutions for wind pressures in which a

model of the structure is subjected to a wind flow profile in an artificially built wind tunnel domain. The current research was conducted as a first step toward using numerical simulation to examine the wind influence on the roofs of a model structure. The time averaged Reynold's Average Navier Stokes (RANS) equations of continuity and momentum were investigated in this work by using the Ansys CFX solver with the usual  $k - \epsilon$  turbulence model. It is the most basic type of numerical simulation, requiring boundary conditions similar to natural conditions. RANS differential equations are solved along with discretized domain and bluff body elements, and the procedure is repeated several times. The flow parameter results may be viewed, and post-result data can be collected. The same process can be done in wind tunnel experiments also, but it is time consuming and the cost of experiment also increases.

Since the effects of wind loading on a structure are unique and wind flow behaves according to the structure's profile, the wind loads show varying patterns on different localized areas on the faces and roof of buildings. Various studies, both analytical, as well as numerical, have been done on different types of structures. Blackmore [1], Gerhardt & Kramer [2], Meecham [3] and Mehta et al. [4] have carried out Wind Flow measurements on actual low-rise buildings of different shapes, and side ratios and have found that small modifications in the edges and shapes of the walls largely impact the wind flow.

Amin and Ahuja[5], Paul and Dalui [6], Mallick et al. [7], Bhattacharyya et al. [8], Chakraborty et al. [9], Mukherjee et al. [10], Bairagi and Mukherjee [11], Sanyal and Dalui [12,13], Kumar and Raj [14] and Gaur and Raj [15] have worked on high rise buildings of various shapes like L, T, Z, C, E, +, N, Y, Octagonal-Oval, etc. by using experimental as well as numerical studies. It has been found that different plan shapes result in altogether different wind pressure patterns.

Singh and Roy [16-19] have worked on CFD simulation on wind effects over Pyramidal Roofs and have studied the effect of wind direction and roof slope for single and double storied pyramidal roof buildings. Rani and Ahuja [20,21], Roy et al. [22], Sakib et al. [23] have studied Canopy roofs subjected to wind loads by using Wind Tunnel Testing. Verma and Ahuja [24] and Zhou, et al. [25] have studied wind effects on Dome structures, which provided a unique shape of the roofs, using wind tunnel tests CFD analysis respectively. Verma and Ahuja [26] have studied the effect of cylindrical roofs in single span as well as double span configurations.

Ahmad and Kumar [27] have studied interference effects on wind load for hip roofs by conducting wind tunnel tests. Significant enhancements and shielding effects were observed for different configurations. Stathopoulos [28] and Stathopoulos et al. [29] have studied the effect of a tall nearby building on the wind loading of low buildings and also carried out wind tunnel tests to examine the effect of the location of trees in the vicinity of

a low-rise building. Significant changes in wind pressures were observed. Tecele et al. [30] have studied the Opening and Compartmentalization Effects of Internal Pressure in Low-Rise Buildings with Gable and Hip Roofs. Gaur et al. [31] have worked on the interference effect on corner configured structures using CFD for different geometry and blockage configurations.

In this paper, a comparative study between Pitched Roof and Arch Roof over a low-rise rectangular plan building was performed using CFD simulations performed under the standard  $k-\epsilon$  turbulence model for high turbulence intensity in the Ansys CFX fluid flow package. It is a preliminary examination of wide span low-rise structures for determining the suitability of use of Ansys CFX. For this study, an arbitrary dimension of the structure has been taken. The calculations of pressure, force, moment, drag and lift coefficients for the models were used for comparison and polynomial mathematical modules were developed between the average pressure coefficient ( $C_p$ ) values and the wind incidence angles were established which can be used to find average  $C_p$  values and corresponding pressures and forces for arbitrary wind incidence angles.

## 2. Simulation Model and Discretization of Computational Domain

For the analysis, a structure with a 1 m x 0.6 m plan area, and 0.5 m wall height is considered as shown in Figures 1 and 2. The pitched roof is inclined at an angle of  $20^\circ$  with the horizontal which results in a maximum elevation of 0.6092 m at the center of the roof. For comparison with an arch roof, a circular arch is considered as a roof that has the same central elevation. The models are created with a wall thickness of 0.01 m and one side of the models is kept open, in order to subject the structure to internal wind pressure also. A scale of 1:10 has been adopted in this study for the scope of future experimental verification.

Equations (1) and (2) represent the profile of the pitched roof and circular arch roof:

$$z = 0.6092 - 0.364|x| \quad (1)$$

$$z = 0.1425 + \sqrt{0.4667^2 - x^2} \quad (2)$$

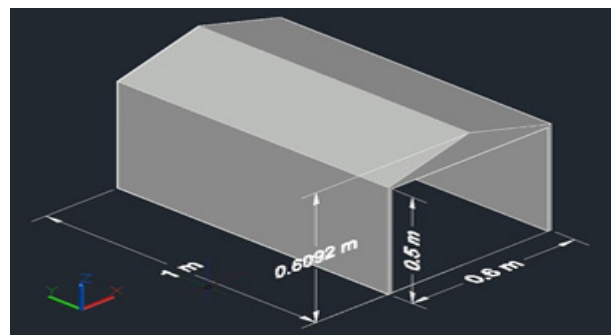


Figure 1. Pitched Roof Model

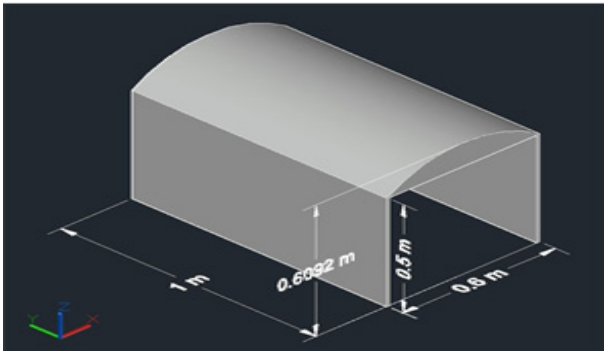


Figure 2. Circular Arch Roof Model

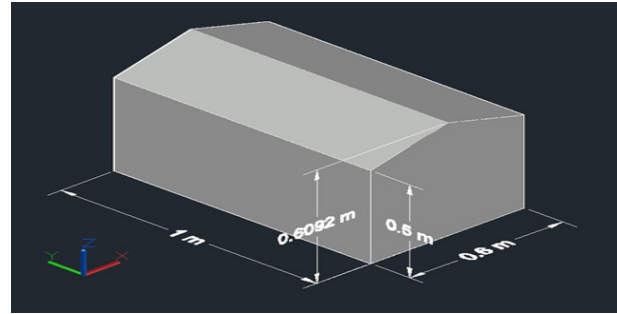


Figure 3. Validation Model

The process of simulation in Ansys CFX requires the creation of discretized flow domain around the geometry and involves the setup for natural boundary conditions which are solved through numerical simulations to get the results. Before the actual simulation, the flow setup and the discretized volume mesh need to be validated against standard wind code provisions. For validating the flow setup, a validation model without opening from one side of the same plan area and height as shown in Figure 3 was subjected to a uniform homogeneous wind flow of 10 m/s at the inlet of the domain since the considered structure is low-rise and the wind flow around the structure is the part of Atmospheric Surface Layer, where the velocity profile can be treated as a uniform profile for simplicity in the analysis. In the validation as well as simulation models, Roof Surface A and B are the windward and leeward sides of the roof as shown in Figure 4.

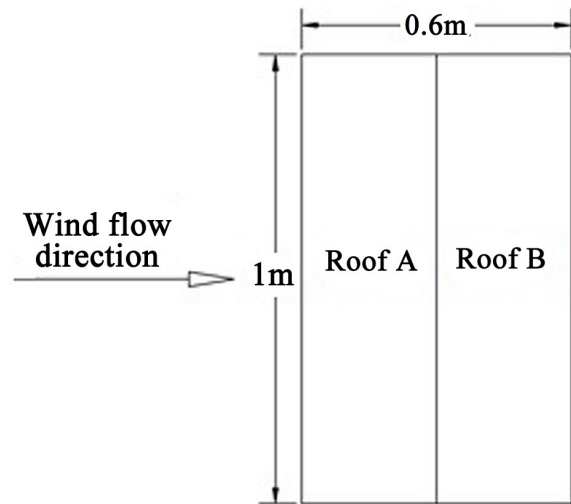


Figure 4. Orientation of Validation Model

After a number of trials, the size for the domain volume mesh grid was finalized as 0.2 m and the model faces and roof meshing sizes as 0.05 m; much smaller as the focus in the present study is to map the pressure effect on the roofs of the model. A diagrammatical representation of the grid size variation is shown in Figure 5. Free slip walls were used to define the domain sides and top for which no shear stress is acting at the wall surface but the velocity along the wall surface has a finite value. The component of wind velocity normal to the wall surface, on the other hand, is zero. The ground and the faces of the model were defined as no slip walls imply that the component of wind velocity along the wall's boundary is zero. The outlet was defined as a boundary having 0 Pa relative pressure.

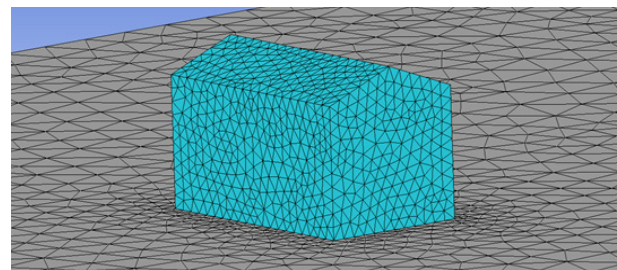


Figure 5. Validation Model - Mesh Diagram

According to Franke et al. [32], the computational domain for the simulation has an optimum size so that the fluid interaction with the model is not harmed by reflection of fluid flow from the domain boundary. For this, the blockage ratio offered by the bluff body should remain below 3%. As a result, the intake and outlet distances from the nearest surface of the model should be kept at 5H and 15H, respectively, and the sides of the domain from the side faces of the model and the top clearance from the model roof should be kept as 5H where H represents the model's maximum height. Using these recommendations, a domain was created for the simulation as shown in Figure 6.

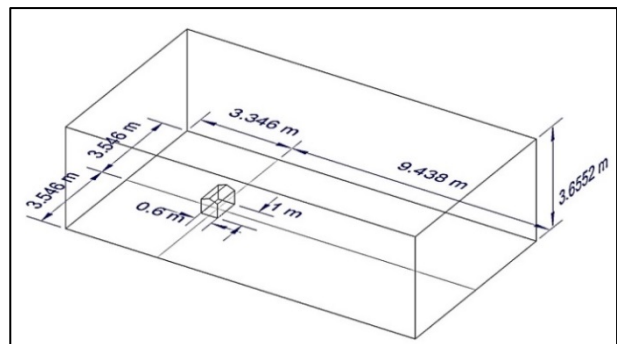
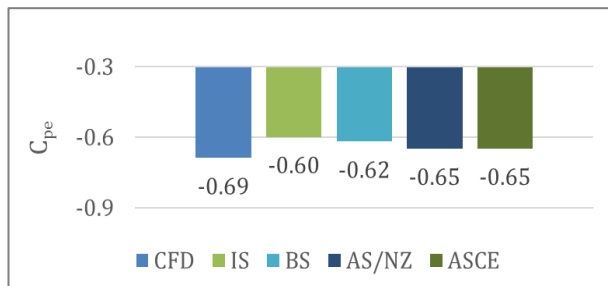


Figure 6. Validation Model - Geometry Setup

The face average value of pressure coefficient obtained

on the validation model was compared with the values given in Indian, British, Australian/ New Zealand, and ASCE standards and the average % variation was found to be 16.5 %, 12.3%, 7.5%, and 7.5% respectively. It can be seen from Figure 7 that the coefficient of pressure values in various international codes/standards deviate from each other and CFD values are within reasonable bounds of 15 to 20%.

For experimental verification, comparison has been made with results available through the wind tunnel tests carried out by Ozmen et al. on pitched roofs to study the effect of roof pitch on the mean pressure coefficient along the mid-axis of building models [33]. The structure considered for the experimental verification has 100mm x 50mm external dimensions with a 15° roof pitch angle with a wall height of 40 mm and a geometric scale of 1:100. The geometric parameters closely match with that considered in the numerical modeling. The data inferred from the graph of the experimental study shows the mean pressure coefficient ( $C_{pe}$ ) for the roof faces to be approximately -0.65. This is in close agreement with the numerical simulation result.



**Figure 7.** Comparison of  $C_{pe}$  obtained with Standard  $C_{pe}$  values given by different Wind Codes

Once the flow setup and discretization of the flow domain were validated, the models were subjected to the same wind flow setup with a similar CFD grid. The wind incidence angles were varied from -90° to 0° (clockwise rotation) and +90° to 0° (anticlockwise rotation) at an interval of 30° with 0° direction along the positive x axis which is normal to the symmetric axis of the building as shown in Figure 8.

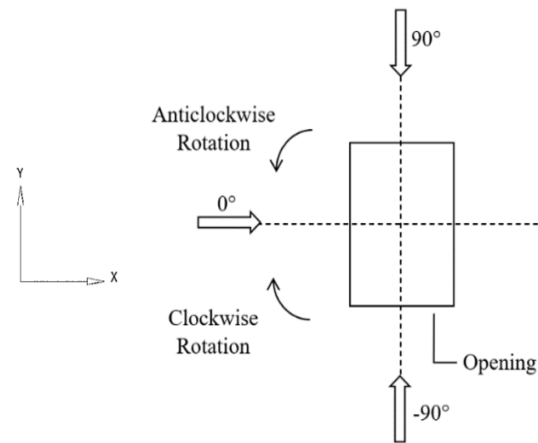


**Figure 8.** Model Orientation

The further sections deal with the calculations of pressure, force, moment, drag and lift coefficients for the models for comparison.

### 3. Pressure Coefficients

Pressure Coefficient is a dimensionless quantity which provides a numerical representation for the relative pressure at any point w.r.t the design pressure. It is defined as shown in (3).

$$\text{Pressure Coefficient} = C_p = \frac{\text{Pressure}}{\frac{1}{2} \cdot \rho \cdot V^2} \quad (3)$$

where,  $\rho$  &  $V$  are the density of air and design wind speed respectively.

The  $C_p$  is a point specific value, which is calculated at the vertices of each node in Ansys CFX. If the surface in consideration is external or internal, the corresponding values of pressure coefficients are represented as  $C_{pe}$  or  $C_{pi}$  respectively and the average pressure coefficient on the surface is represented as  $C_{pe(avg)}/C_{pi(avg)}$ . The maximum pressure coefficient,  $C_{pe(max)}/C_{pi(max)}$ , and the minimum pressure coefficient,  $C_{pe(min)}/C_{pi(min)}$ , at a point on the surface are critical for design of roof elements and supporting structures and fixtures. Based on equation (3), the contours of  $C_p$  for the roof surfaces in this study are shown in the following figures.

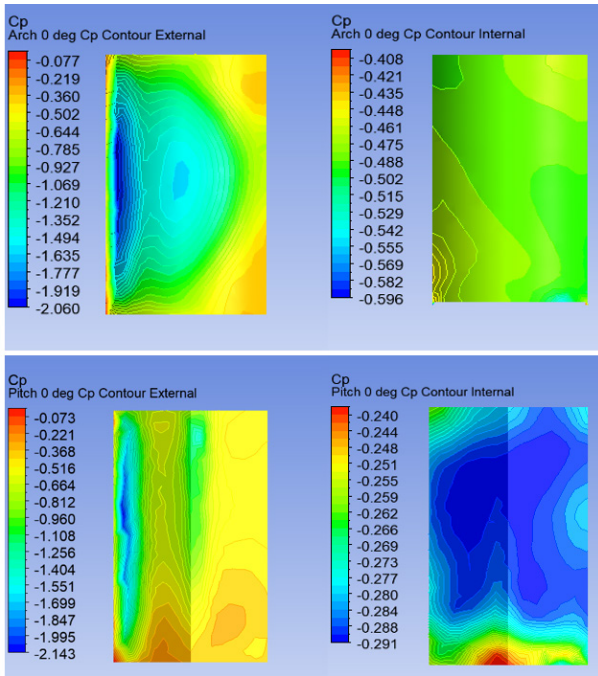


Figure 9.  $C_p$  Contours for 0° Wind Incidence

For a 0° wind incidence, Figure 9 depicts the  $C_p$  contours for the external and internal faces of the Arch and Pitch roofs. The  $C_{pe}$  is negative for both the pitched and arch roofs, with a slight rise in the  $C_{pe(min)}$  for the pitched roof. This is due to the sharp edge of the pitch roof's rooftop, which causes eddies on the leeward side of the roof, producing increased suction. In this case, the effect of vortex shedding is easily noticeable. The  $C_{pi}$  contour for both roofs has a uniform nature, with the pitched roof having a smaller magnitude of suction  $C_{pi}$  values than the arch roof which is due to the presence of a planar roof surface that gives more resistance to air circulation in the internal environment.

The  $C_p$  contours in Figures 10, 11, 12 and 13 are obtained corresponding to the wind incidences at +30°, +60° & -30°, -60°. For +30°, higher magnitudes of  $C_{pe}$  as well as  $C_{pi}$  are observed than the corresponding values for +60°, for both the roofs. This is due to the higher blockage offered by the structures to the wind flow in 30° configuration. The same trend is observed for  $C_{pe}$  in -30° and -60° configurations also. However, this trend reverses for  $C_{pi}$  in -30° and -60°, since the internal pressures in these cases are governed by the direct wind entry in the internal environment and -60° configuration offers a more exposed opening to the wind flow.

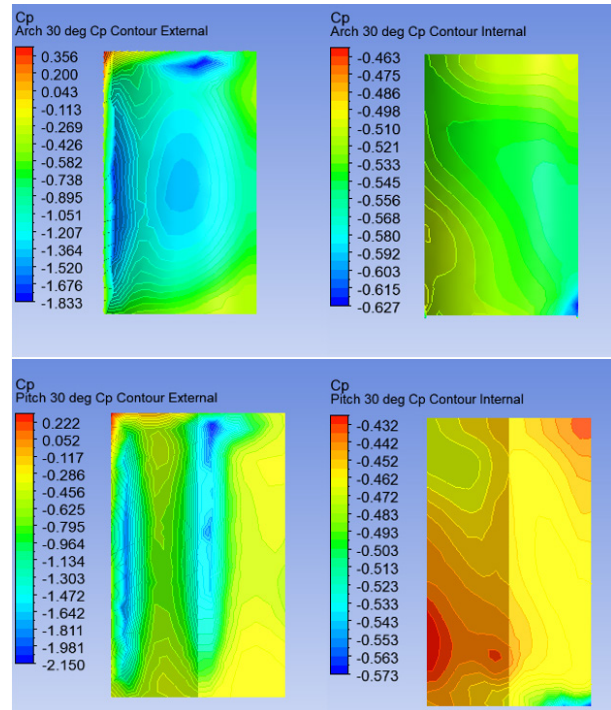


Figure 10.  $C_p$  Contours for 30° Wind Incidence

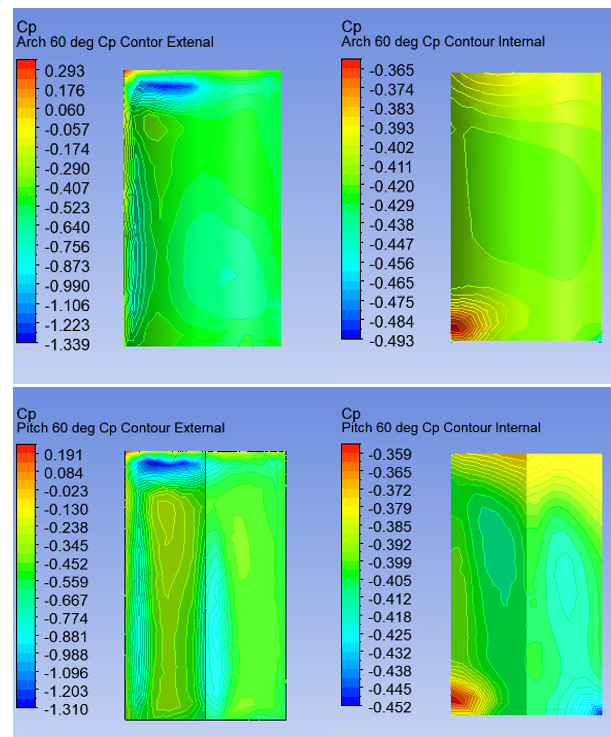


Figure 11.  $C_p$  Contours for 60° Wind Incidence

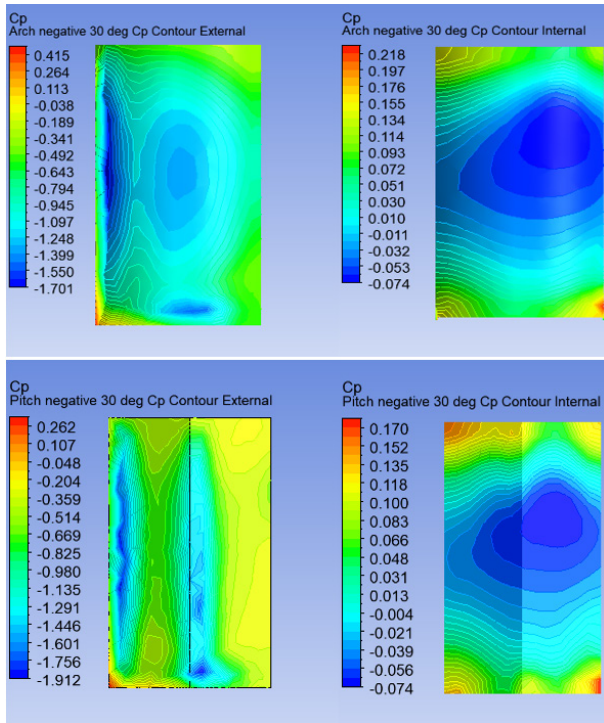


Figure 12.  $C_p$  Contours for  $-30^\circ$  Wind Incidence

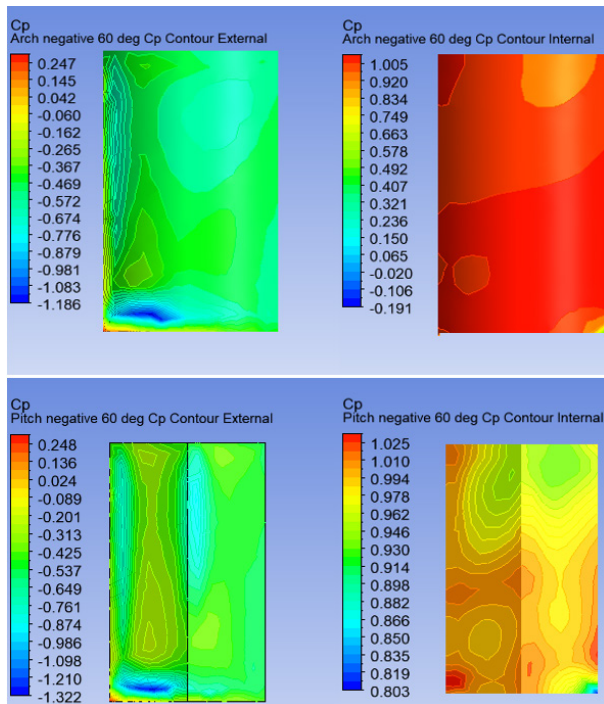


Figure 13.  $C_p$  Contours for  $-60^\circ$  Wind Incidence

If the arch and pitched roofs are compared among themselves, the  $C_{pi}$  does not show significant variation. However,  $C_{pe(max)}$  for arch roofs are about 1.75 times that for a pitched roof. The surfaces of arch roofs have more elevation due to their convex upwards nature, which results in more blockage to the wind flow. On the other hand,  $C_{pe(min)}$  shows the opposite trend as the suction on the external roof is caused by the flow separation, which

occurs more for the pitched roof due to its sharp roof top, thus causing more suction.

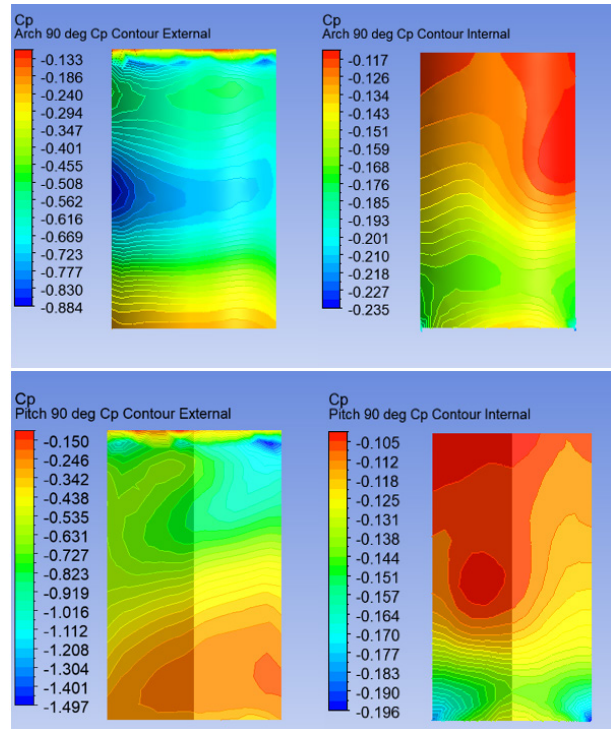


Figure 14.  $C_p$  Contours for  $90^\circ$  Wind Incidence

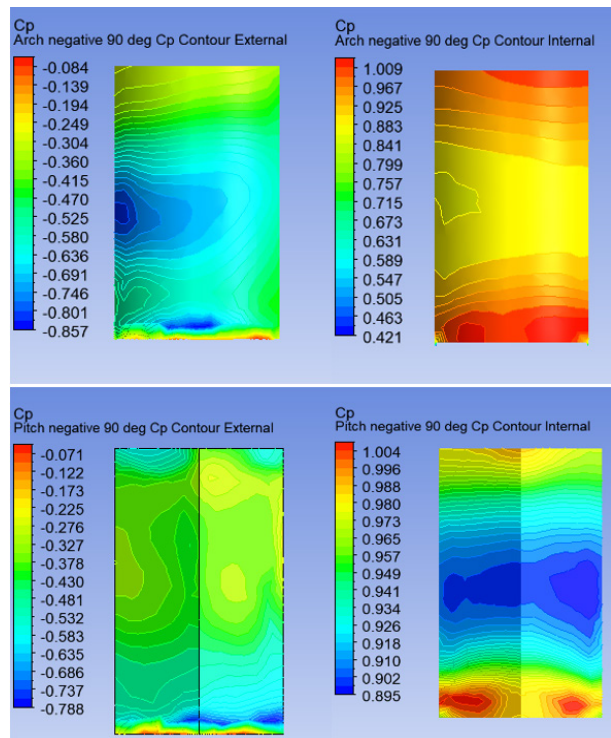


Figure 15.  $C_p$  Contours for  $-90^\circ$  Wind Incidence

The  $C_p$  contours in Figures 14 and 15 are obtained corresponding to the wind incidence for  $+90^\circ$  and  $-90^\circ$ , respectively. These scenarios depict the building's closed

and open sides with relation to the domain inlets, respectively. For both wind incidences, the contour variation for  $C_{pe}$  of both roofs shows negative values throughout the roof surface. Due to the bluff body nature of the pitched roof and the splitting of the wind streamline at the rooftop, the  $C_{pe(min)}$  value for the external roof faces for both wind incidence angles are higher for the pitched roof.

The values of  $C_{pi}$  are having smaller magnitudes and are causing suction for  $+90^\circ$  wind incidence since the wind circulates in the internal environment after losing a significant amount of velocity due to the presence of a closed wall on the windward side. However, the same is

positive for  $-90^\circ$  because of the outward pressure exerted on the internal roof face due to the opening in the structure being on the windward side. The  $C_{pi(max)}$  values for both pitched and arch roof internal surfaces are identical (1.009 and 1.004 respectively), but the  $C_{pi(min)}$  value for the  $-90^\circ$  wind incidence is nearly twice in the pitched roof case due to the pitched roof's sharp edge and planar surface.

The maximum, minimum and average  $C_p$  were plotted for the External and Internal Roof Surfaces for both the structures for different wind incidence angles to study the variation of pressure coefficients for each roof surface as shown in Figures 16 to 21.

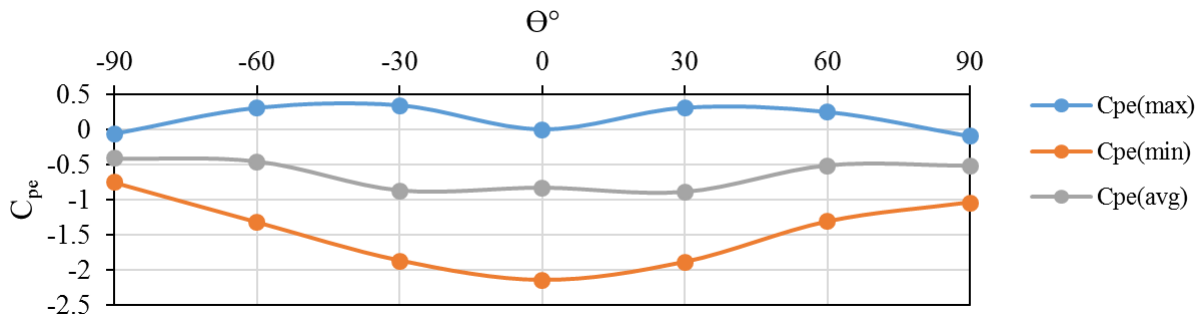


Figure 16. Pitched Roof A - External Coefficient of Pressure ( $C_{pe}$ ) v/s Wind Incidence Angle ( $\Theta^\circ$ )

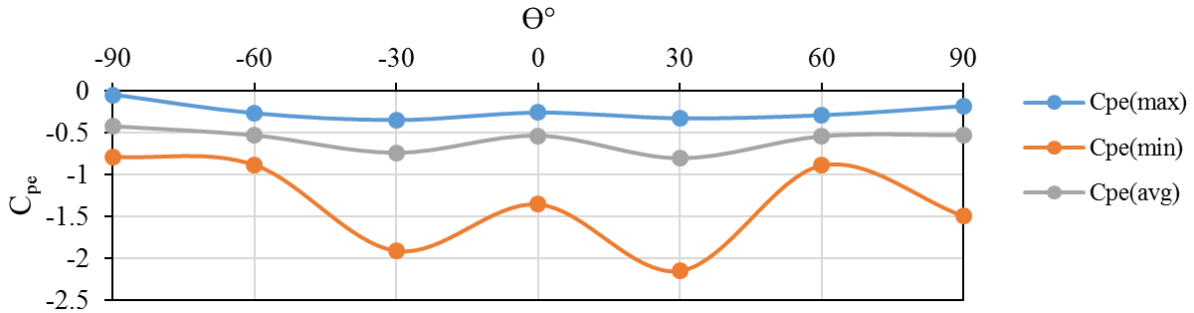


Figure 17. Pitched Roof B - External Coefficient of Pressure ( $C_{pe}$ ) v/s Wind Incidence Angle ( $\Theta^\circ$ )

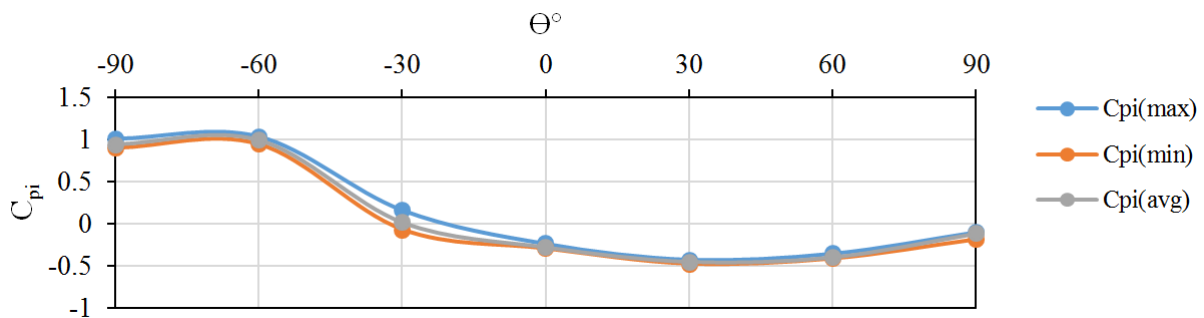


Figure 18. Pitched Roof A - Internal Coefficient of Pressure ( $C_{pi}$ ) v/s Wind Incidence Angle ( $\Theta^\circ$ )

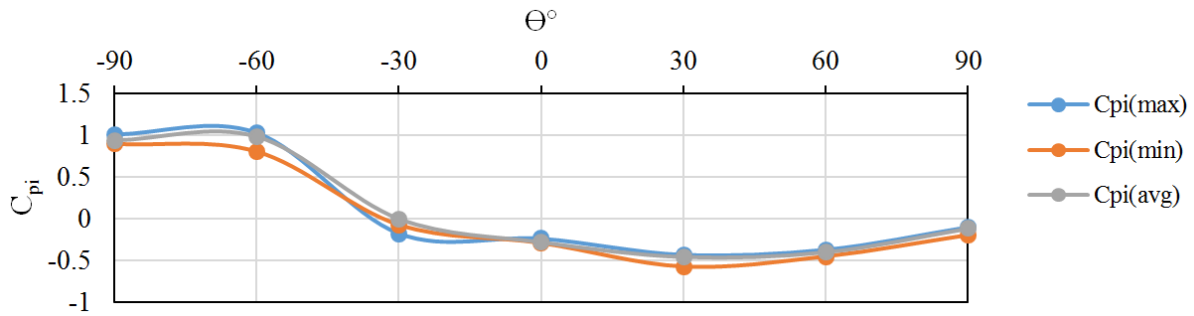


Figure 19. Pitched Roof B - Internal Coefficient of Pressure (C<sub>pi</sub>) v/s Wind Incidence Angle (Θ°)

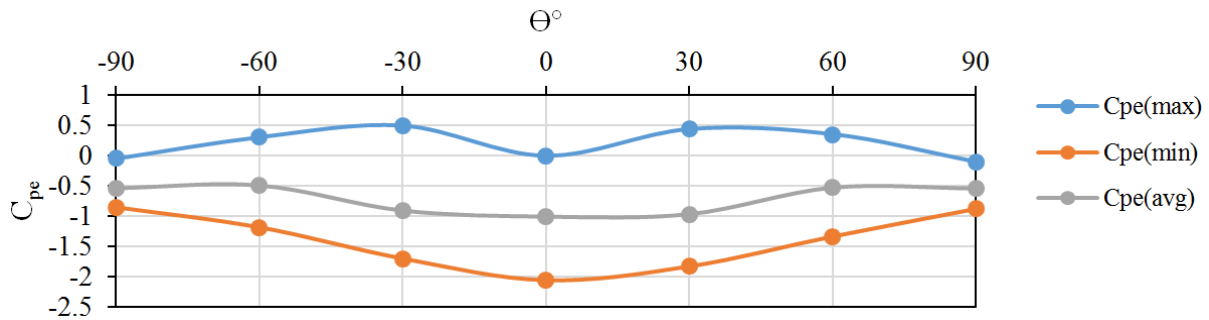


Figure 20. Arch Roof - External Coefficient of Pressure (C<sub>pe</sub>) v/s Wind Incidence Angle (Θ°)

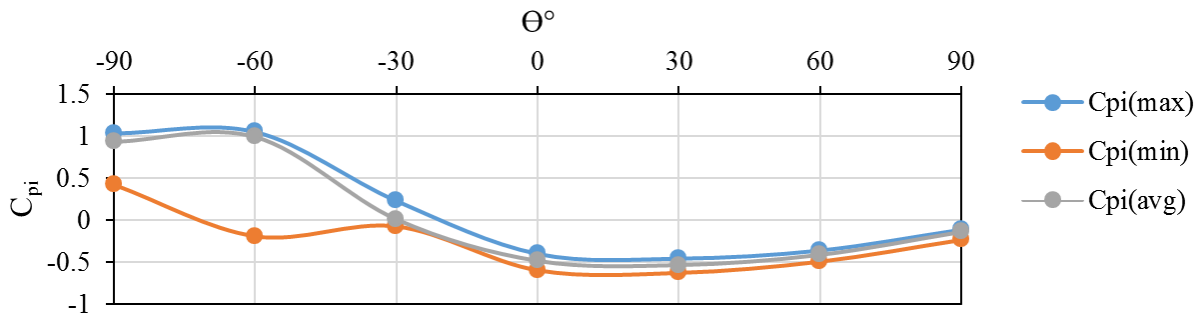


Figure 21. Arch Roof - Internal Coefficient of Pressure (C<sub>pi</sub>) v/s Wind Incidence Angle (Θ°)

There is a symmetry about 0° wind incidence angle for the C<sub>p(avg)</sub>, C<sub>p(max)</sub>, and C<sub>p(min)</sub> graphs of external faces for both the roof types with the value of C<sub>p(avg)</sub> increasing for the pitched roof by nearly 1.2 times at 0° wind incidence because of its sharp edge. The nature of the C<sub>p</sub> graphs for the internal faces is also similar for both the roofs. However, there is no symmetry about the 0° wind incidence angle as the effect of closed and open walls becomes more eminent for the internal roof faces. The average C<sub>p</sub> values of the internal faces for both roofs are almost identical in this case.

#### 4. Force, Moment, Drag and Lift Coefficients

Force Coefficients (C<sub>fx</sub>, C<sub>fy</sub>, C<sub>fz</sub>) as shown in (4), (5), and (6) and Moment Coefficients (C<sub>mx</sub>, C<sub>my</sub>, C<sub>mz</sub>) as shown in (7), (8) and (9) are important parameters for the

design of buildings and roofs against wind loadings. These coefficients provide a platform to compare the behavior of the structures against wind. They can be applied to prototype building for calculating resultant forces and moments acting on the buildings in different directions. The drag and lift coefficients (C<sub>d</sub> and C<sub>l</sub>) as shown in (10) and (11) are the force coefficients in the direction along and perpendicular to the direction of wind flow. These coefficients were calculated for the different incidence angles of wind for the study of the two roofs.

$$C_{fx} = \frac{F_x}{\frac{1}{2} \rho V^2 L_y H} \tag{4}$$

$$C_{fy} = \frac{F_y}{\frac{1}{2} \rho V^2 L_x H} \tag{5}$$

$$C_{fz} = \frac{F_z}{\frac{1}{2} \rho V^2 L_x L_y} \tag{6}$$

$$C_{mx} = \frac{M_x}{\frac{1}{2} \rho V^2 L_x H^2} \tag{7}$$

$$C_{my} = \frac{M_x}{\frac{1}{2} \rho V^2 L_y H^2} \tag{8}$$

$$C_{mz} = \frac{M_x}{\frac{1}{2} \rho V^2 L_x L_y H} \tag{9}$$

$$C_d = \frac{F_{along}}{\frac{1}{2} \rho V^2 L_y H} \tag{10}$$

$$C_l = \frac{F_{across}}{\frac{1}{2} \rho V^2 L_x H} \tag{11}$$

**Table 1.** Projected Lengths of the buildings about x and y directions

Angle	L <sub>x</sub> (m)	L <sub>y</sub> (m)
0°	0.6	1
±30°	1.0196	1.1660
±60°	1.1660	1.0196
±90°	1	0.6

where, ρ & V are the density of air and wind velocity respectively; L<sub>x</sub> is the projected length along wind direction and L<sub>y</sub> is the projected length across wind direction which depend on the orientation of the model as described in Table 1; H is the maximum height of the model (=0.6092 m); F<sub>x</sub>, F<sub>y</sub>, F<sub>z</sub> & M<sub>x</sub>, M<sub>y</sub>, M<sub>z</sub> are the sum of the forces and moments induced on all the faces of the building along the x, y and z directions; F<sub>along</sub> and F<sub>across</sub> are the forces on the building along the wind direction and perpendicular (across) wind direction respectively.

Figures 22 and 23 represent the variation of coefficients of forces along the different directions w.r.t the wind incidence angles for the two buildings. The nature of the graphs is almost similar for both the roof types and symmetry about the 0° wind incidence angle can also be seen for the C<sub>fx</sub> graph. However, the values of C<sub>fx</sub> and C<sub>fy</sub> are slightly lower (0.133 and 0.78 times respectively) at 0° wind incidence angle for the arch roof building as compared to the pitched roof because of its plane and continuous roof top.

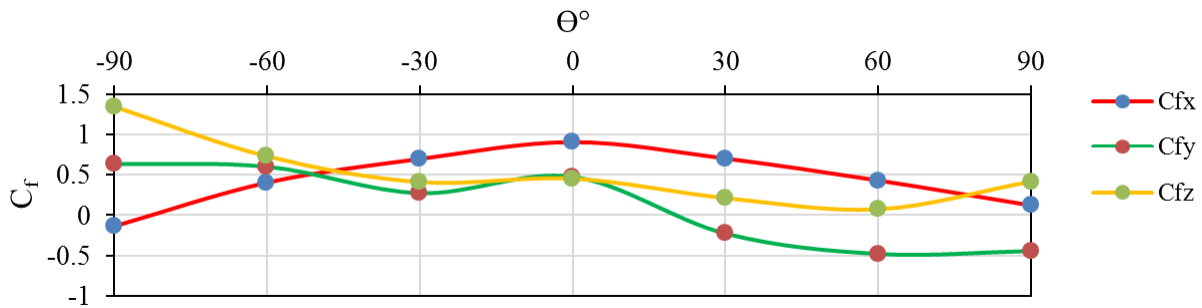


**Figure 22.** Pitched Roof - Force Coefficient (C<sub>f</sub>) v/s Wind Incidence Angle (Θ°)

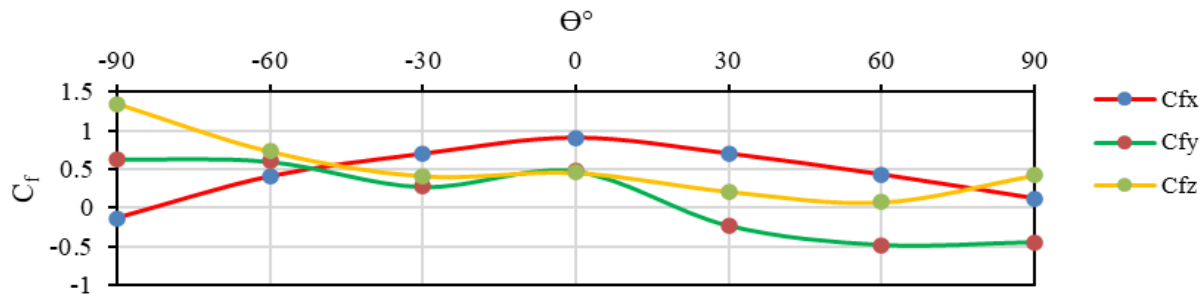


**Figure 23.** Arch Roof - Force Coefficient (C<sub>f</sub>) v/s Wind Incidence Angle (Θ°)

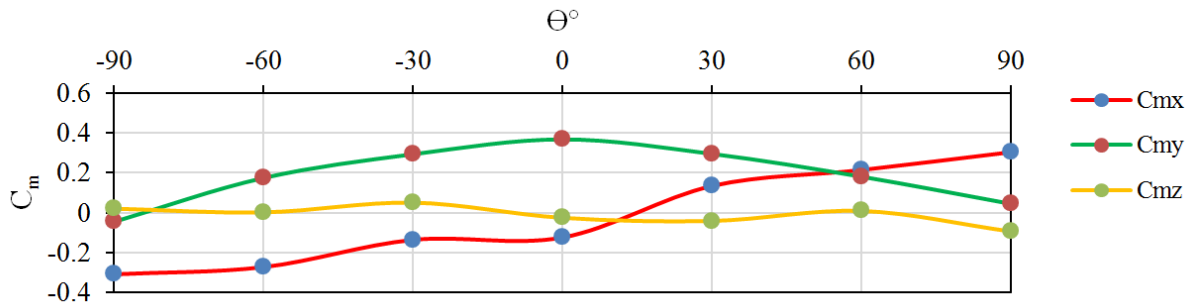


**Figure 24.** Pitched Roof - Moment Coefficient (C<sub>m</sub>) v/s Wind Incidence Angle (Θ°)

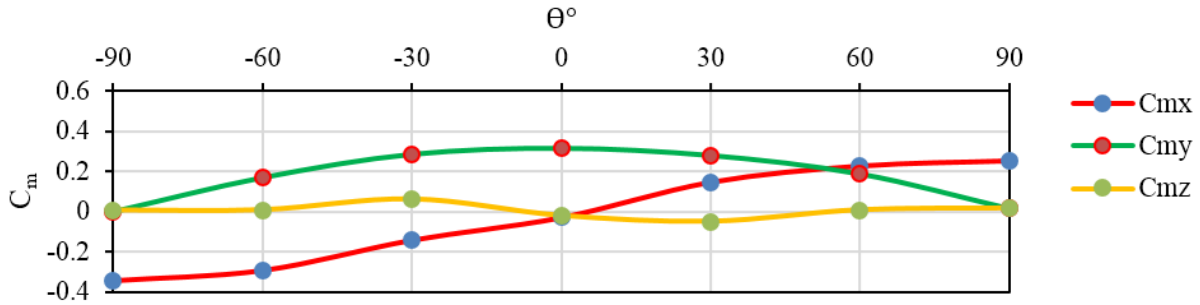


Figure 25. Arch Roof - Moment Coefficient (C<sub>m</sub>) v/s Wind Incidence Angle (Θ°)

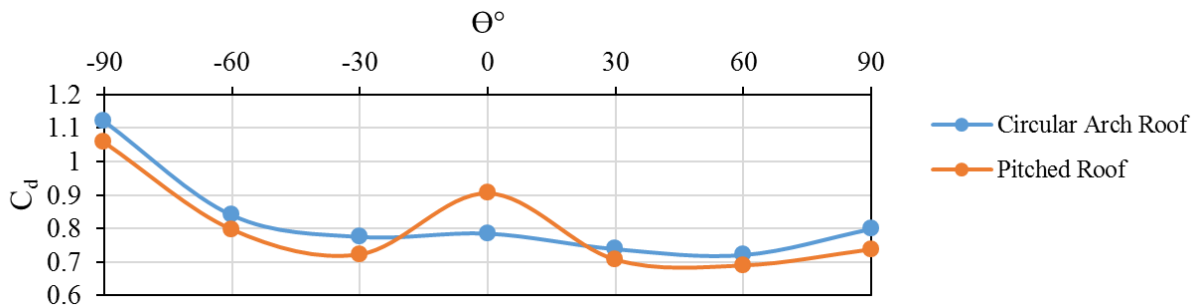


Figure 26. Drag Coefficient (C<sub>d</sub>) v/s Wind Incidence Angle (Θ°)

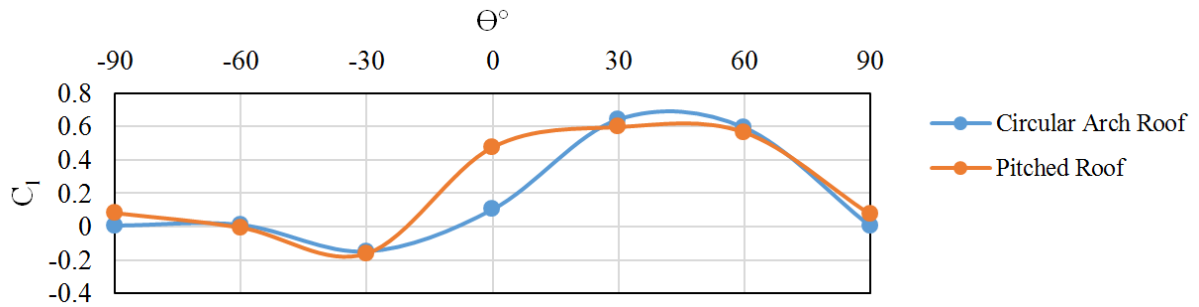


Figure 27. Lift Coefficient (C<sub>l</sub>) v/s Wind Incidence Angle (Θ°)

Figures 24 and 25 represent the variation of coefficients of moments along the different directions w.r.t the wind incidence angles for the two buildings. The nature of the graphs is similar for both the roof types and symmetry about the 0° wind incidence angle can also be seen for each of the C<sub>mx</sub>, C<sub>my</sub> and C<sub>mz</sub> graphs. The magnitude of the data points is also somewhat similar for the C<sub>my</sub> and C<sub>mz</sub> graphs however a decrease in the C<sub>mx</sub> value by nearly 4 times can be seen at the 0° wind incidence angle for the pitch roof building as compared to the arch roof. It is also observed that there exists a resemblance in the C<sub>fx</sub>, C<sub>my</sub> graph and C<sub>fy</sub>, C<sub>mx</sub> graph respectively in terms of their nature. This occurs because of the similar variables in their equations.

Figures 26 and 27 represent the coefficient of drag and lift for the two roof types w.r.t the wind incidence angles. The nature of both C<sub>d</sub> and C<sub>l</sub> graphs is almost similar with very slight differences in magnitudes at the different wind incidence angles for both the roof types, however a significant increase in the values of both C<sub>d</sub> and C<sub>l</sub> is seen at 0° for the pitch roof building (by nearly 1.15 and 4.60 times respectively) and this happens because of its sharp

roof edge which induces a larger force in the along wind direction (drag) and splits the wind streamline for a larger wind force in the across direction (lift).

### 5. Mathematical modules between C<sub>pe(avg)</sub>/C<sub>pi(avg)</sub> and Wind Incidence Angle

The C<sub>pe(avg)</sub>/C<sub>pi(avg)</sub> face average values of pressure coefficients are important to study the behavior of the roof under wind load as other parameters such as pressures and forces could be easily estimated once these values are obtained. However, the process to obtain these values for different wind incidence angles on Ansys CFX is a tedious and cumbersome process, since the software reiterates from the beginning. Thus, a standard relationship established between the C<sub>pe(avg)</sub>/C<sub>pi(avg)</sub> values and the wind incidence angles is of great use. Here the available values of C<sub>pe(avg)</sub>/C<sub>pi(avg)</sub> for the seven wind incidence angles

through the simulations conducted are utilized to establish polynomial relations. These polynomial relations are developed by studying the nature of the  $C_{pe(avg)}/C_{pi(avg)}$  graphs for both the external and internal faces of both the roofs and are given in Table 2. The coefficients are solved through the use of the available boundary conditions ( $C_{pe(avg)}/C_{pi(avg)}$  values of different wind incidence angles) and verified through their trendline plots. Suitable periods of angles are classified so as to satisfy the nature of the curve variation.

## 6. Conclusion and Future Work

A comparison of a pitched roof and a circular arch roof low-rise structure has been made in this study. Both types of roofs are common in the industry, and they feature similar frontal projections. When the building's dimensions and slope of the roofs are kept constant, the shape and curvature of the roofs govern the wind load response. The opening on one side of the building causes the external and interior roof faces to behave differently.

While the sharp edges of the pitch roof produce slight increase in suction on external roof for the  $0^\circ$ , it is observed that the clockwise rotation of the building with respect to the wind causes an increase in  $C_{pi}$  values for both roofs,

corresponding to larger exposed opening to the wind and with higher magnitudes for the pitched roof due to its sharp edge. The anticlockwise rotations, on the other hand, produce negative  $C_{pe}$  and  $C_{pi}$  values, with the arch roof having a larger magnitude than the pitched roof.

The force and moment coefficients computed along the x, y and z directions show similar nature for both roofs with symmetries about the  $0^\circ$  wind incidence for these coefficients. However, a lower value of  $C_{fx}$  and  $C_{fy}$  is observed for the arch roof than in pitched roof. This is because the velocity sharply escapes the sharp roof edge and vortex shedding becomes more eminent in the pitched roof which leads to a relatively higher magnitude of suction force in the pitched roof, which increases the forces in the horizontal plane.

The drag coefficient ( $C_d$ ) and lift coefficient ( $C_l$ ) show similar variation for both roofs, but the magnitudes are significantly higher for the pitched roof, especially at  $0^\circ$  wind incidence angle. This roof's sharp-edged roof top is again responsible for the increase in coefficients due to better wind streamline splitting.

The relations established between the  $C_{pe(avg)}/C_{pi(avg)}$  values and the wind incidence angles in polynomial form can be of great use for quicker estimation of average pressure coefficient, pressures, and forces on both the external and internal faces of both the roofs.

**Table 2.** Equations for  $C_{pe(avg)}/C_{pi(avg)}$  in terms of  $\theta$  (in radians)

Roof	Equation for $C_{pe(avg)}/C_{pi(avg)}$ in terms of $\theta$ (in radians)	Range for $\theta$
Arch Roof External Face	$C_{pe(avg)} = -0.027\theta - 0.5040$	$\theta \in [-90^\circ, -60^\circ]$ & $[60^\circ, 90^\circ]$
	$C_{pe(avg)} = 0.0482\theta^3 + 0.4816\theta^2 - 0.0702\theta - 1.0113$	$\theta \in [-60^\circ, 60^\circ]$
Arch Roof Internal Face	$C_{pi(avg)} = -0.110\theta - 1.1040$	$\theta \in [-90^\circ, -60^\circ]$
	$C_{pi(avg)} = -0.1606\theta^3 + 0.6938\theta^2 - 0.4874\theta - 0.483$	$\theta \in [-60^\circ, 90^\circ]$
Pitched Roof External Face A	$C_{pe(avg)} = -0.6733\theta^2 - 1.8423\theta - 1.6497$	$\theta \in [-90^\circ, -30^\circ]$
	$C_{pe(avg)} = -0.1775\theta^2 - 0.0201\theta - 0.8316$	$\theta \in [-30^\circ, 30^\circ]$
	$C_{pe(avg)} = -0.6952\theta^2 + 1.8105\theta - 1.6482$	$\theta \in [-30^\circ, 90^\circ]$
Pitched Roof Internal Face A	$C_{pi(avg)} = 0.096\theta + 1.096$	$\theta \in [-90^\circ, -60^\circ]$
	$C_{pi(avg)} = 0.1544\theta^4 - 0.288\theta^3 + 0.376\theta^2 - 0.3539\theta - 0.2802$	$\theta \in [-60^\circ, 90^\circ]$
Pitched Roof External Face B	$C_{pe(avg)} = -0.1813\theta^2 - 0.683\theta - 1.0484$	$\theta \in [-90^\circ, -30^\circ]$
	$C_{pe(avg)} = -0.8594\theta^2 - 0.0619\theta - 0.5373$	$\theta \in [-30^\circ, 30^\circ]$
	$C_{pe(avg)} = -0.4497\theta^2 + 1.2049\theta - 1.3129$	$\theta \in [30^\circ, 90^\circ]$
Pitched Roof Internal Face B	$C_{pi(avg)} = 0.088\theta + 1.073$	$\theta \in [-90^\circ, -60^\circ]$
	$C_{pi(avg)} = 0.1646\theta^4 - 0.3016\theta^3 + 0.3636\theta^2 - 0.3371\theta - 0.2833$	$\theta \in [-60^\circ, 90^\circ]$

The results and conclusions established in this study have direct implications on similar studies on the other roof types and varied width to span ratios. This comparative study provides key insights on the difference created by the shape and curvature of the roof on the pressure, force, moment, drag and lift coefficients which can be extended to other families of roofs. This will be beneficial in the study of the structural soundness of the roof types under wind load conditions, accompanied by an economic design. This study can be extended towards high-speed wind conditions also. The relationship developed between the  $C_{pe(avg)}/C_{pi(avg)}$  values and wind incidence angle can also be extended to develop relationships between the wind incidence angles and the other coefficients (force, moment, drag, lift) which can help in deciding the best suited roof among the different families of roofs.

## Acknowledgments

The authors would like to thank the Department of Civil Engineering, Delhi Technological University for providing the required training and research support for conducting the simulations on Ansys Software.

---

## REFERENCES

- [1] P. A. Blackmore. Load reduction on flat roofs - the effect of edge profile, *Journal of Wind Engineering and Industrial Aerodynamics*, Vol. 29, No. 1, pp. 89–98, 1988.
- [2] H. J. Gerhardt and C. Kramer. Effect of building geometry on roof wind loading, *Journal of Wind Engineering and Industrial Aerodynamics*, Vol. 43, No. 1, pp. 1765–1773, 1992.
- [3] D. Meecham. The improved performance of hip roofs in extreme winds — A case study, *Journal of Wind Engineering and Industrial Aerodynamics*, Vol. 43, No. 1, pp. 1717–1726, 1992.
- [4] K. C. Mehta, M. L. Levitan, R. E. Iverson, and J. R. McDonald. Roof corner pressures measured in the field on a low building, *Journal of Wind Engineering and Industrial Aerodynamics*, pp. 181–192, 1992.
- [5] J. A. Amin and A. K. Ahuja. Experimental study of wind-induced pressures on buildings of various geometries, 2011.
- [6] R. Paul and S. K. Dalui. Wind effects on ‘Z’ plan-shaped tall building: a case study, *International Journal of Advanced Structural Engineering*, vol. 8, no. 3, pp. 319–335, 2016.
- [7] M. Mallick, A. Kumar, and K. C. Patra. Experimental Investigation on the Wind-Induced Pressures on C-Shaped Buildings, *KSCE Journal of Civil Engineering*, Vol. 23, No. 8, pp. 3535–3546, 2019.
- [8] B. Bhattacharyya, S. K. Dalui, and A. K. Ahuja. Wind Induced Pressure on ‘E’ Plan Shaped Tall Buildings, *Jordan Journal of Civil Engineering*, Vol. 8, No. 2, p. 120, 2014.
- [9] S. Chakraborty, K. Dalui, and A. K. Ahuja. Experimental Investigation of Surface Pressure on ‘+’ Plan Shape Tall Building, *Jordan Journal of Civil Engineering*, Vol. 8, No. 3, p. 251, 2014.
- [10] S. Mukherjee, S. Chakraborty, S. K. Dalui, and A. K. Ahuja. Wind induced pressure on ‘Y’ plan shape tall building, *Wind and Structures, An International Journal*, Vol. 19, No. 5, pp. 523–540, 2014.
- [11] K. Bairagi and A. Mukherjee. Wind pressure and velocity pattern around ‘N’ plan shape tall building - A case study, *Asian Journal of Civil Engineering*, Vol. 18, No. 8, pp. 1241–1258, 2017.
- [12] P. Sanyal and S. K. Dalui. Effects of internal angle between limbs of ‘Y’ plan shaped tall building under wind load, *Journal of Building Engineering*, Vol. 33, 2021.
- [13] P. Sanyal and S. K. Dalui. Effects of side ratio for ‘Y’ plan shaped tall building under wind load, *Building Simulation*, Vol. 14, No. 4, pp. 1221–1236, 2021.
- [14] Kumar and R. Raj. Study of Pressure Distribution on an Irregular Octagonal Plan Oval-Shape Building Using CFD, *Civil Engineering Journal*, Vol. 7, No. 10, 2021.
- [15] N. Gaur and R. Raj. Aerodynamic mitigation by corner modification on square model under wind loads employing CFD and wind tunnel, *Ain Shams Engineering Journal*, 2021.
- [16] J. Singh and A. K. Roy. Effects of roof slope and wind direction on wind pressure distribution on the roof of a square plan pyramidal low-rise building using CFD simulation, *International Journal of Advanced Structural Engineering*, Vol. 11, No. 2, pp. 231–254, 2019.
- [17] J. Singh and A. K. Roy. CFD simulation of the wind field around pyramidal roofed single-story buildings, *SN Applied Sciences*, Vol. 1, No. 11, 2019.
- [18] J. Singh and A. K. Roy. Wind Pressure Coefficients on Pyramidal Roof of Square Plan Low Rise Double Storey Building, *Computational Engineering and Physical Modeling*, Vol. 2, No. 1, pp. 1–16, 2019.
- [19] J. Singh and A. K. Roy. Wind loads on roof of low-rise buildings, *Disaster Advances*, Vol. 14, No. 5, pp. 83–98, 2021.
- [20] N. Rani and A. K. Ahuja. Wind Loads on Multi-Span Mono-Slope Canopy Roof, in *Urbanization Challenges in Emerging Economies*, pp. 702–708, 2017.
- [21] N. Rani and A. K. Ahuja. Wind Loads on Flat Canopy Roofs, 2017.
- [22] K. Roy, A. K. Ahuja, and V. K. Gupta. Variation of Wind Pressure on Canopy-Roofs, *International Journal of Earth Sciences and Engineering*, Vol. 3, No. 2, pp. 19–30, 2010.
- [23] F. A. Sakib, T. Stathopoulos, and A. K. Bhowmick. A review of wind loads on canopies attached to walls of low-rise buildings, *Engineering Structures*, Vol. 230, 111656, 2021.

- [24] Verma and A. K. Ahuja. Wind Pressure Distribution on Rectangular Plan Buildings with Multiple Domes, *International Journal of Engineering and Technical Research (IJETR)*, Vol. 3, No. 7, pp. 129–133, 2015.
- [25] P. Zhou, B. Tang, P. Liu, and G. Zheng. Study on Wind Load Distribution on the Surface of Dome Structure Based on CFD Numerical Simulation, in *Journal of Physics: Conference Series*, Vol. 1176, No. 5, 2019.
- [26] Verma and A. K. Ahuja. Wind Pressure Distribution on Low-Rise buildings with Cylindrical Roofs, in *Implementing Innovative Ideas in Structural Engineering and Project Management*, pp. 1211–1216, 2015.
- [27] S. Ahmad and K. Kumar. Interference effects on wind loads on low-rise hip roof buildings, *Engineering Structures*, Vol. 23, No. 12, pp. 1577–1589, 2001.
- [28] T. Stathopoulos. Adverse Wind Loads on Low Buildings Due to Buffeting, *Journal of Structural Engineering*, Vol. 110, No. 10, pp. 2374–2392, 1984.
- [29] T. Stathopoulos, D. Chiovitti, and L. Dodaro. Wind shielding effects of trees on low buildings, *Building and Environment*, Vol. 29, No. 2, pp. 141–150, 1994.
- [30] S. Tecele, G. T. Bitsuamlak, and A. G. Chowdhury. Opening and Compartmentalization Effects of Internal Pressure in Low-Rise Buildings with Gable and Hip Roofs, *Journal of Architectural Engineering*, Vol. 21, No. 1, 04014002, 2015.
- [31] N. Gaur, R. Raj, and P. K. Goyal. Interference effect on corner-configured structures with variable geometry and blockage configurations under wind loads using CFD, *Asian Journal of Civil Engineering*, 2021.
- [32] J. Franke et al. Recommendations on the use of CFD in wind engineering, *Proceedings of the International Conference on Urban Wind Engineering and Building Aerodynamics*. 2004.
- [33] Y. Ozmen, E. Baydar, and J. P. A. J. van Beeck. Wind flow over the low-rise building models with gabled roofs having different pitch angles, *Building and Environment*, Vol. 95, pp. 63–74, 2016.